ECS Transactions, 78 (1) 387-394 (2017)
10.1149/07801.0387ecst ©The Electrochemical Society

Low Temperature Synthesis and Properties of Gadolinium-Doped Cerium Oxide Nanoparticles

M. F. S. Machado[a], L. P. R. Moraes[a], N. K. Monteiro[a], V. Esposito[b], D. Z. de Florio[c], D. Marani[b] and F. C. Fonseca[a]

[a] Instituto de Pesquisas Energéticas e Nucleares, IPEN
São Paulo, SP, 05508000, Brazil
[b] Department of Energy Conversion and Storage, Technical University of Denmark
Frederiksborgvej 399, 4000, Roskilde, Denmark
[c] Universidade Federal do ABC, Santo André, SP, 09219170, Brazil

Gadolinium-doped cerium oxide (GDC) is an attractive ceramic material for solid oxide fuel cells (SOFCs) both as the electrolyte and in composite electrodes operating at low and intermediate temperatures. GDC exhibits high oxygen ion conductivity at a wide range of temperatures and displays a high resistance to carbon deposition when hydrocarbons are used as fuels. However, an inconvenience of ceria-based oxides is the high sintering temperature needed to obtain a fully dense ceramic body. In this study, a green chemistry route for the synthesis of 10 mol% GDC nanoparticles is proposed. The aqueous precipitation method starts from the nitrates of both cerium and gadolinium and uses excess hexamethylenetetramine (HMT) to produce crystalline GDC at 80 ºC. Such a low temperature synthesis provides control over particle size and sinterability of the material at low temperatures.

Introduction

Ceria-based electrolytes have been studied extensively as alternative electrolytes for intermediate temperature (600-800 °C) solid oxide fuel cells (SOFC) with 10% gadolinium-doped cerium oxide (GDC) being the most attractive candidate (1). GDC has also showed potential as an anode material in fuel flexible SOFCs, for the internal steam reforming of hydrocarbon and alcohol fuels avoiding the deposition of carbon in the anodes (2-4). At intermediate temperatures Ce^{4+} reduces to Ce^{3+} creating defects as oxygen vacancies and induces n-type conductivity in reducing atmospheres. This reduction can be aided by the introduction of an aliovalent dopant such as Gd_2O_3, increasing the chemical stability and forming a solid solution. The ionic radius of the dopant is similar to the radius of Ce^{4+} introducing vacancies in the network as charge compensation defects. High ionic conductivity is due to oxygen vacancies and an electronic conductivity of n-type in reducing atmospheres is important for anodic materials (5-7). The morphology of the starting powder of the doped ceria greatly affects its physical chemical properties and require tailoring to be processed as a component of a SOFC (8).

A disadvantage of the synthesis of ceria-based oxides is the high sintering temperature required to obtain a fully dense ceramic body, above 1500 °C for several

hours or having to use sintering aids (9, 10). These high temperatures, besides representing a costlier process, can promote unwanted reactions between the components of the fuel cell (11). Sinterability can be improved with optimized densification and minimized grain growth by using better starting powders (12). Several chemical methods have been presented which aim to increase sinterability by developing homogeneous, reactive and ultrafine GDC powder (13). The most promising techniques are the sol-gel route (10, 14), the Pechini method (15), precipitation (16-18) and hydrothermal synthesis (13).

In this work simple aqueous homogeneous precipitation method was adapted from Chen et al (19) to produce nanocrystalline highly reactive GDC powder. The method starts from the nitrates of cerium and gadolinium and use excess hexamethylenetetramine (HMT) to control the rate of precipitation and ensure that the reaction goes to completion. Hydrolysis occurs slowly at low temperature such that the precipitates are formed uniformly and simultaneously within the solution. The effect of aging the solution before heating was studied. This low temperature synthesis results in nanometric GDC powders, which can be sintered to full density at temperatures below 1500°C.

Experimental

Two different routes were used to synthesize 10% gadolinium-doped cerium oxide (GDC). In both methods cerium nitrate hexahydrate (Aldrich, 99,99%), gadolinium nitrate hexahydrate (Aldrich, 99,99%) and HMT (Vetec, 99%) were used. In the fast method (-f) the reactants were heated and stirred at 80 °C for 3 h. The precipitate was washed in the centrifuge with water and isopropyl alcohol and dried in the oven at 80 °C for 12 h. In the aging method (-a) the aqueous solution was allowed to react at room temperature for 12 h before following the same heating, washing and drying procedure as the fast route.

X-ray diffraction and thermogravimetric analyzes of the obtained powders were performed. The materials were characterized by X-ray diffraction (XRD) using a Rigaku diffractometer model Miniflex II and source of Cu Kα radiation. The crystallite size was calculated using Scherrer's equation. Thermogravimetric (TG) analyzes were done using Setaram Labsys equipment, between room temperature and 1400 °C with a heating rate of 10 °C min^{-1} under synthetic air flow.

The materials were calcined at 500°C for 1 h in air. Cylindrical pellets were prepared by uniaxial pressing for dilatometry analysis. Setaram Labsys equipment was used in the same conditions as in the TG analysis. Cylindrical pellets were sintered at 1400°C for 2 h and at 1500°C for 1 h. Apparent densities of the pellets were measured using the Archimedes principle and the theoretical densities of each sample were calculated to obtain the relative density.

The electrical properties of the material were analyzed by impedance spectroscopy with a Solartron frequency analyzer (SI 1260) in the frequency range 10 MHz to 1 Hz and 100 mV ac amplitude. Measurements were performed in the 200°C - 600°C temperature range in static air. The electrical contacts were made by painting the parallel surfaces of the sintered pellets with silver paint followed by curing at 600°C for 1 h.

Topographical analysis of the polished and thermally attacked surfaces of the pellets was carried out using a Scanning Probe Microscope (SPM) JEOL 5200.

Results and Discussion

X-ray diffractograms (XRD) of GDC (Figure 1) showed diffraction peaks corresponding to a $Ce_{0.9}Gd_{0.1}O_{1.95}$ (JCPDS 75-0161). All diffraction patterns confirm the formation of the cubic crystalline structure of the fluorite type. The fast synthesis resulted in a crystalline material without the presence of impurities prior to any heat treatment, whereas in the aged reaction the XRD of the as-synthesized powder shows the presence of by-products. This indicates that the fast synthesis has a greater control over the reaction and that it was completed in the period of 3 h. After calcination, both methods resulted in a single-phase material.

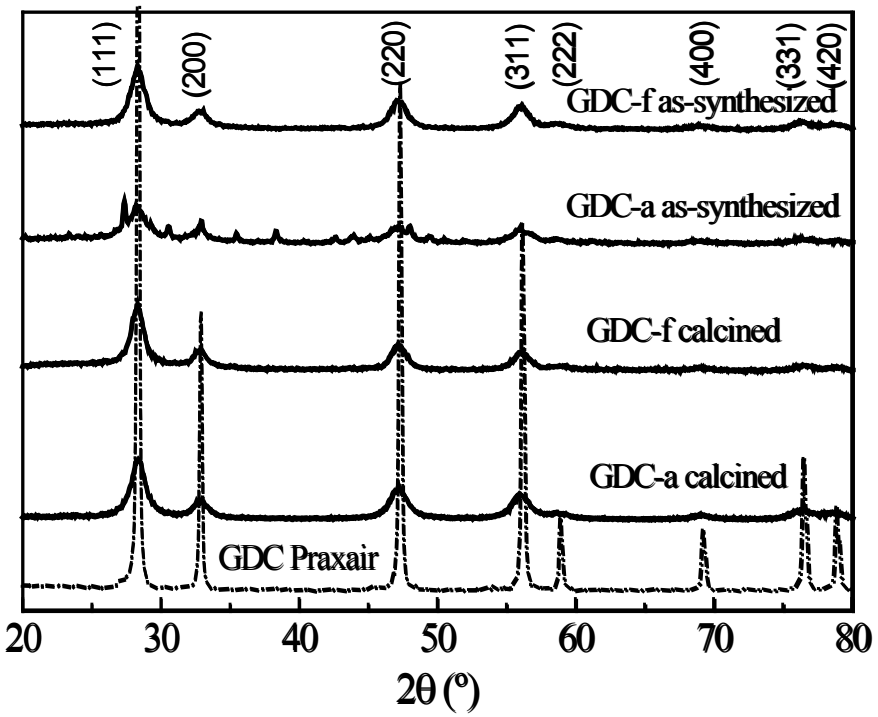

Figure 1. X-ray diffraction patterns of GDC synthesized by the fast and aging methods before any heat treatment and calcined. Commercial GDC is shown for comparison.

The average crystallite sizes were determined from the XRD data from the full-width half-maximum (FWHM) of the most intense peak according to Scherrer's equation. The mean crystallite size for the calcined GDC was ~7 nm, whereas for the commercial 10% GDC (Praxair 99.9% purity, 0.4 μm particle size) the crystallite size calculated was 39 nm.

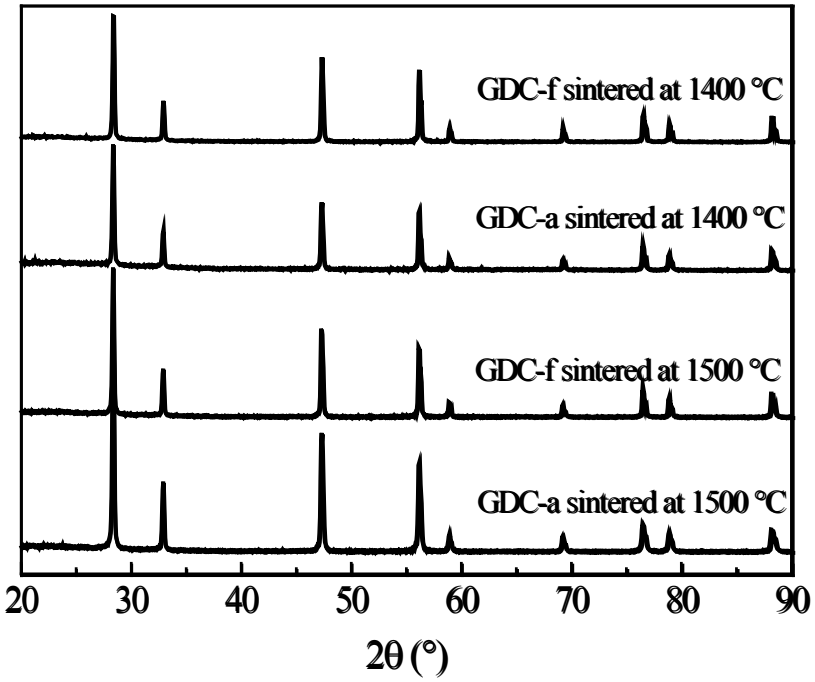

Figure 2. X-ray diffraction patterns of GDC synthesized by the fast and aging methods sintered at 1400 °C and 1500°C.

The XRD patterns of the samples sintered at 1400°C and 1500°C are shown in Figure 2. The calculated lattice parameters from the XRD data was ~5.45 Å for all samples including the commercial GDC.

The thermogravimetric analysis (TGA) of the as-synthesized powders is shown in Figure 3.

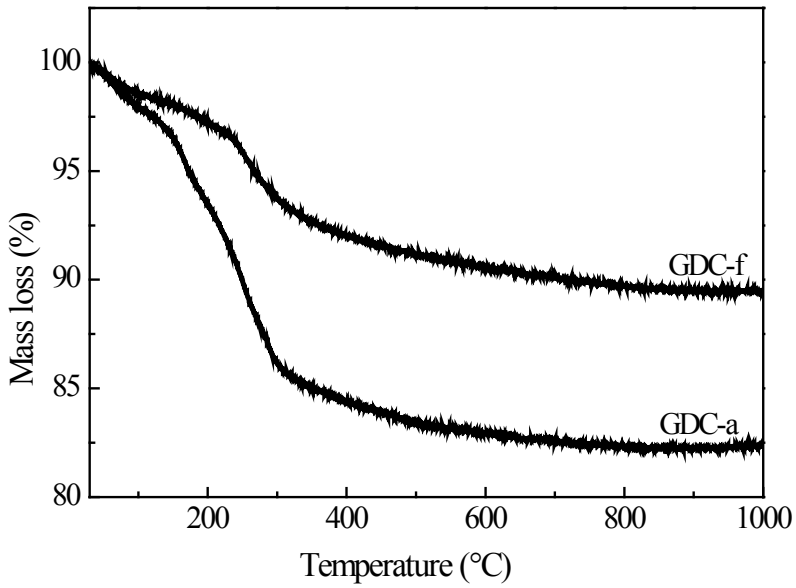

Figure 3. Thermogravimetric analysis of GDC synthesized by the fast and aging methods.

The main mass loss occurs at temperatures < 400 °C. For both synthesis methods, the TGA curve shows an initial loss of trapped humidity and above 200 °C the organic compounds are decomposed. The total mass loss of GDC-f was of ~ 10%, whereas GDC-

a had a mass loss of ~ 17%. The larger mass loss for GDC-a indicates impurities in the powder corresponding to a larger amount of organics, in agreement with the XRD,

Dilatometry analysis of the calcined powders (Figure 4) and of the commercial GDC (Praxair) powder was carried out. The relative green densities were ~ 50% for the synthesized pellets and ~ 60% for the commercial GDC. The dilatometry curves of the synthesized samples show continuous retraction starting from 600°C to 1400°C and total retraction > 20%. The profiles of the samples did not show densification plateaus indicating that sintering is not complete at 1400°C. On the other hand, the GDC-a and the GDC-f samples showed much higher sinterability with a large shrinkage and an onset of densification at temperatures as low as 600°C, much lower than the one of commercial GDC (~900°C) (20). A deeper analysis on the sintering activity of samples was carried out by calculating the differential shrinkage as function of the temperature (Fig. 3b). As

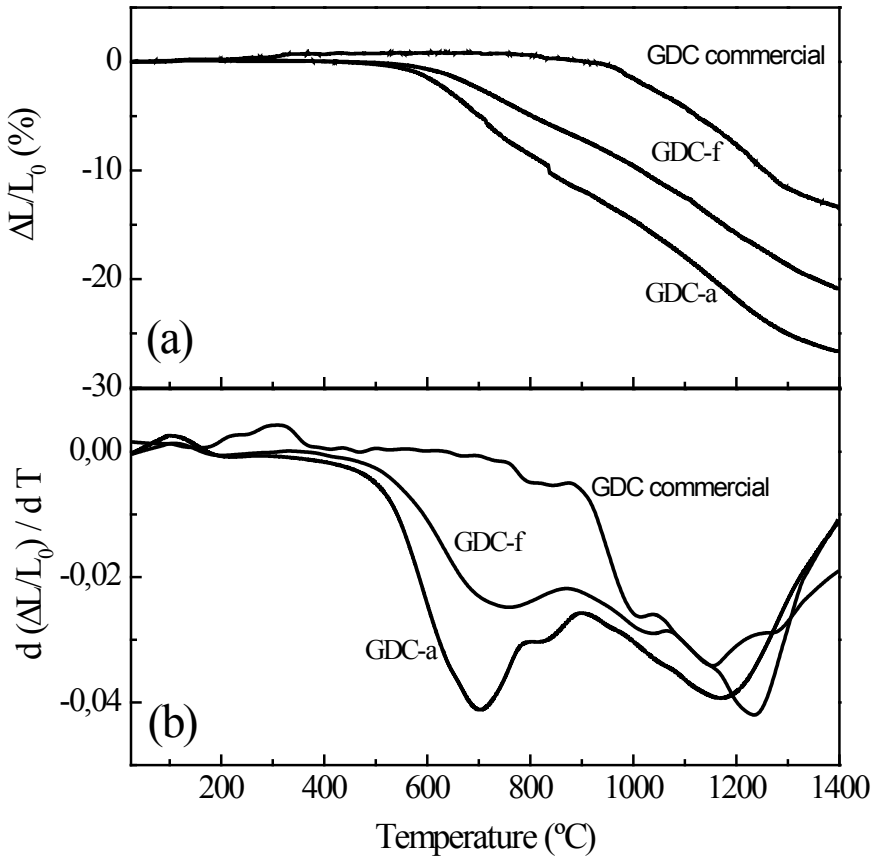

Figure 4. (a) Dilatometric analysis of GDC synthesized by the fast and aging methods after calcination at 500 °C. (b) Temperature dependence of the derivative of the sintering curve.

the dilatometry curves were measured at constant heating rates, their derivatives correspond to the sintering rates of the samples, which reflects microstructural and compositional features of the synthesized powders (21). All samples show multi-step sintering effects, but with rather different densification behaviour. Commercial GDC shows inhibited sintering processes up to ~900°C and maximum sintering activity at ~1250°C. Such features suggest large initial particle size in which surface diffusion mechanisms are limited with respect to lattice diffusion (21). Conversely, the GDC-a sample shows a clear two-step sintering with a first maximum sintering activity at 700 °C

and a second step at 1200°C. The GDC-f sample shows similar behaviour but with a lower total activity. The fast densification at low temperature can be attributed to the high surface energy in the nanometric powders that leads to a fast sintering at low temperature (~700°C), achieving ~50% of the densification (Fig. 3a). The high temperature (~1200°C) maximum sintering activity indicates a full activation of lattice diffusion mechanisms in nanometric powders leading to the final sintering stage.

The hydrostatic apparent density of pellets sintered at 1400°C and 1500°C were calculated using the Archimedes principle and the theoretical densities of the samples were obtained from XRD estimated lattice parameter. Based on the hydrostatic density of the samples sintered at 1400°C, a relative density of ~92% was reached. Upon increasing the sintering temperature by 100°C increased the relative density of both samples to ~98%. The results show that aging the solution has a small effect on the densification of the pellets, as aging ensures that an ultrafine and homogeneous powder is slowly precipitated.

The electrical conductivity of GDC-f and GDC-a sintered at 1400°C and at 1500°C was evaluated by impedance spectroscopy measurements. The impedance spectra revealed two semicircles with contributions ascribed to the bulk and grain boundaries, based on differences in relaxation frequency. At temperatures above 300°C the relaxation frequencies of the processes increase, thus separate semicircles due to bulk and grain boundary are not distinguished. Figure 4 shows the impedance spectra of GDC aged sintered at 1400°C and at 1500°C. The semicircle located in the high frequency region (HF) is attributed to the bulk resistance and the second semicircle in the low frequency regions (LF) is attributed to the grain boundary due to residual porosity and impurities. The total resistance of the samples is dominated by the low frequency resistance. Increasing the sintering temperature decreased both high and low frequency components as a result of the increased density.

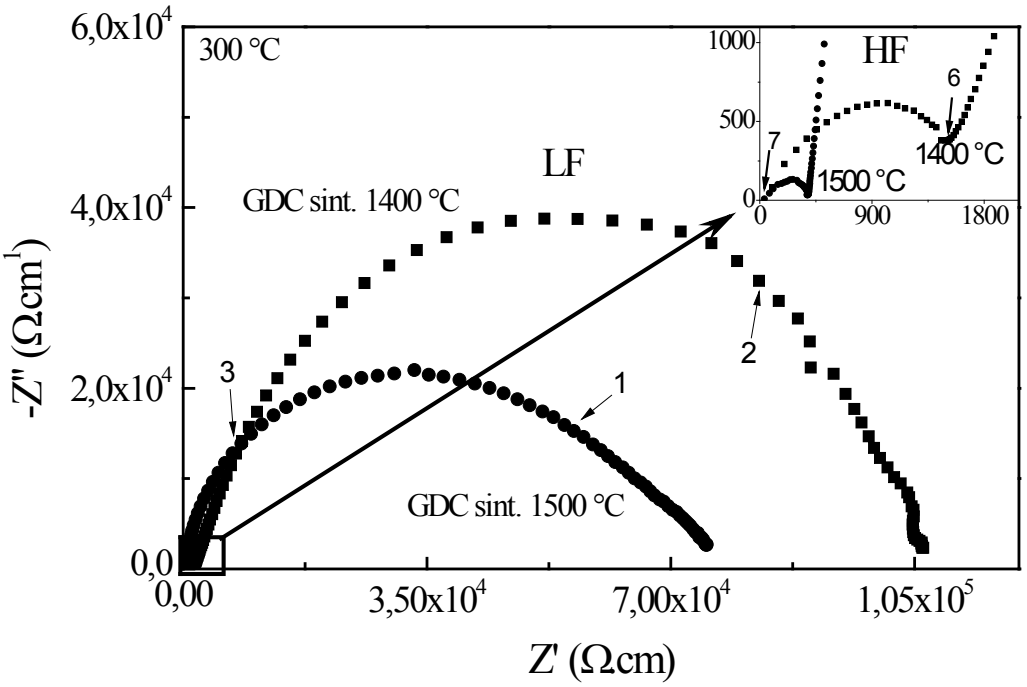

Figure 5. Impedance spectra of GDC pellet synthesized by the aging method sintered at 1400°C and 1500°C.

The Scanning Probe Microscope (SPM) images show the surface of the pellets sintered at 1500°C (Figure 6). From the SPM images it can be noted that both samples have well-defined grains with clean grain boundaries discerned and high density. Average particle size < 1 μm was visually estimated for both samples.

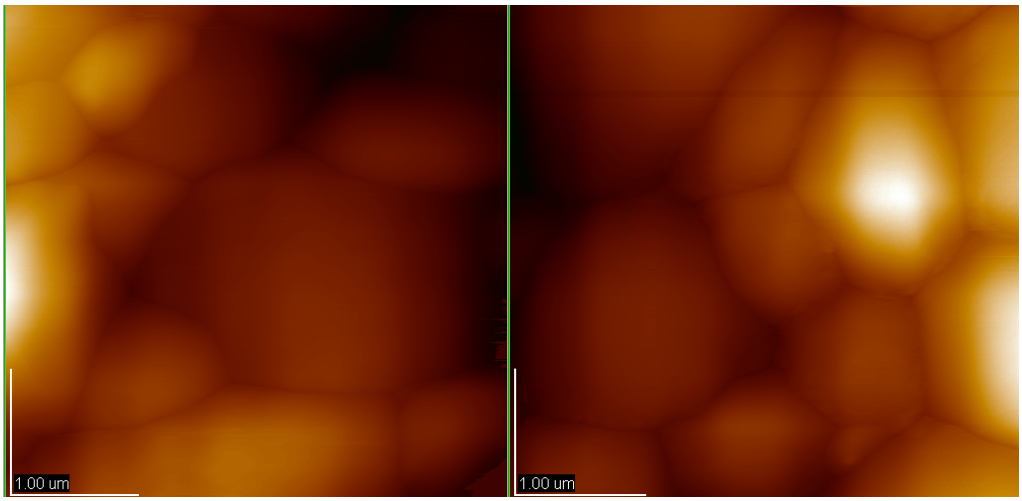

Figure 6. Surface SPM images of fractured pellets sintered at 1500°C through the fast method (left) and the aging method (right).

Conclusions

Nanometric 10 mol% gadolinium-doped cerium oxide was successfully synthesized by a low temperature green chemistry route. The fabricated ceramic exhibited the expected fluorite-type structure with nanometric crystallite sizes, which promoted good densification at relatively low temperatures. Samples prepared by aging the solution before heating presented finer particles with high sinterability resulting in slightly denser ceramics. The electrical conductivity of the samples was greatly affected by the porosity of the pellets, seen as the dominant low frequency resistance. The sintered samples exhibited electrical conductivity comparable to previously reported data for GDC. These results evidenced a facile route for GDC synthesis resulting in a material with the desired properties and high potential for use in solid oxide fuel cells.

Acknowledgments

The authors are thankful for the support of the Brazilian agencies CAPES, CNPq, CNEN and FAPESP (2014/09087-4, 2014/50279-4, 2013/26961-7, 2015/20434-0 and 2016/07156-4). Dr. R. Muccillo (IPEN) is acknowledged for the SPM images.

References

1. A. Atkinson, *Solid State Ion.*, **95**, 249 (1997).
2. A. Atkinson, S. Barnett, R.J. Gorte, J.T.S. Irvine, A.J. Mcevoy, M. Mogensen, S.C. Singhal, J. Vohs, *Nat. Mater.*, **3**, 17 (2004).

3. G. Postole, K. Girona, J. Toyir, A. Kaddouri, P. Gélin, *Fuel Cells*, **12**, 275 (2012).
4. B. L. Augusto, F. B. Noronha, F. C. Fonseca, F. N. Tabuti, R. C. Colman, L. V. Mattos, *Int. J. Hydrog. Energy*, **39**, 11196, (2014).
5. B. Steele, *Solid State Ion.*, **129**, 95, (2000).
6. S. Wang, T. Kobayashi, M. Dokiya, T. Hashimoto, *J. Electrochem. Soc.*, **147**, 3606, (2000).
7. M. Mogensen, *Solid State Ion.*, **129**, 63, (2000).
8. V. Esposito and E. Traversa, *J. Am. Ceram. Soc.*, **91**, 1037 (2008).
9. Z. Gao, D. Kennouche, S. A. Barnett, *J. Power Sources*, **260**, 259, (2014).
10. R. Fuentes and R. Baker, *Int. J. Hydrog. Energy*, **33**, 3480, (2008).
11. V. Esposito De Wei Ni, D. Marani, F. Teocoli, K. T. S. Thydén, D. Z. de Florio, F. C. Fonseca., *J Mater Chem A*, **4**, 16871, (2016).
12. D. Z. de Florio, V. Esposito, E. Traversa, R. Muccillo, F. C. Fonseca, *J. Therm. Anal. Calorim.*, **97**, 143, (2009).
13. D. Marani, V. Esposito, B. R. Sudireddy, J. J. Bentzen, P. S. Jørgensen, D. W. Ni, F. Teocoli, R. Kiebach. *Ceram. Int.*, **43**, 5647, (2017).
14. A. Zarkov A. Stanulis, T. Salkus, A. Kezionis, V. Jasulaitiene, R. Ramanauskas, S. Tautkus, A. Kareiva, *Ceram. Int.*, **42**, 3972, (2016).
15. A. Arabacı and M. F. Öksüzömer, *Ceram. Int.*, **38**, 6509, (2012).
16. D. W. Joh, M. K. Rath, J. W. Park, J. H. Park, K. H. Cho, S. Lee, K. J. Yoon, J. Lee, K. T. Lee, *J. Alloys Compd.*, **682**, 188, (2016).
17. G. Accardo, L. Spiridigliozzi, R. Cioffi, C. Ferone, E. Di Bartolomeo, Sung Pil Yoon, G. Dell'Agli, *Mater. Chem. Phys.*, (187), 149, (2017).
18. M. J. Godinho, R. F. Gonçalves, L. P. S Santos, J. A. Varela, E. Longo, E. R. Leite, *Mater. Lett.*, **61**, 1904, (2007).
19. P. L. Chen and I. W. Chen, *J. Am. Ceram. Soc.*, 76, 1577, (1993).
20. S.Y. Park, C. W. Na, J. H. Ahn, R.-H. Song, J. H. Lee," *J. Asian Ceram. Soc.*, **2**, 339, (2014).
21. D.W. Ni, C. G. Schmidt, F. Teocoli, A. Kaiser, K. B. Andersen, S. Ramousse, V. Esposito, *J. Eur. Ceram. Soc.*, **33**, 2529, (2013).